Block-Copolymer-Templated Ordered Mesoporous Silica: Array of Uniform Mesopores or Mesopore−Micropore Network?

Ryong Ryoo and Chang Hyun Ko

Department of Chemistry and School of Molecular Science (BK21), Korea Advanced Institute of Science and Technology, Taeduk Science Town, Taejon, 305-701 Korea

Michal Kruk, Valentyn Antochshuk, and Mietek Jaroniec*

Department of Chemistry, Kent State University, Kent, Ohio 44240

Received: March 28, 2000

Microporosity and connectivity of ordered mesopores of SBA-15 silica were studied using nitrogen adsorption and novel methods based on selective pore blocking via organosilane modification, and on the imaging of inverse platinum replica of ordered mesoporous structure. It was found that SBA-15 exhibits a relation between the pore size, pore volume and specific surface area which is significantly different from that for cylindrical or hexagonal pores, which suggests that the SBA-15 structure is more complex than an array of hexagonally ordered channels, even if they are corrugated. Nitrogen and argon adsorption measurements provided evidence that large mesopores are accompanied by a certain amount of significantly smaller pores (of the size below about 3.4 nm) with a broad distribution primarily in the micropore/small-mesopore range. The modification of SBA-15 via chemical bonding of small trimethylsilyl ligands partially blocked the complementary pores, and the bonding of larger octyldimethylsilyl groups made them essentially fully inaccessible to nitrogen molecules, which manifested itself in dramatic changes in the relation between the pore size, pore volume, and specific surface area. After dissolution of the SBA-15 framework, platinum wires grown inside the porous structure formed bundles, as seen from transmission electron microscopy. These results provided strong and unambiguous evidence that large ordered mesopores of SBA-15 are accompanied by much smaller disordered pores and that an appreciable fraction of the latter is located in the pore walls, providing connectivity between the ordered large-pore channels. The complementary pores are suggested to form as a result of penetration of poly(ethylene oxide) chains of the triblock copolymer template within the silica framework of as-synthesized SBA-15. We also studied thermal stability of SBA-15 structure and its complementary porosity. As inferred from nitrogen adsorption data, the complementary porosity was retained to a significant extent even after calcination at 1173 K, but most likely completely disappeared at 1273 K. The heat treatment was accompanied not only by a significant decrease in the specific surface area and pore volume but also by narrowing the pore size distribution at temperatures up to 1173 K. Thus, we were able to demonstrate for the first time that the SBA-15 sample with nitrogen adsorption properties similar to those of MCM-41 can be obtained via calcination at 1273 K, although the pore volume and specific surface area of such SBA-15 material is relatively low.

1. Introduction

The opportunities in the synthesis of ordered mesoporous materials discovered in the early nineties[1,2] were remarkably enhanced when it was recognized that oligomers and polymers are facile supramolecular templates.[3−24] Polymeric templates provide vast opportunities in the pore size and pore structure engineering, are inexpensive and can be readily recovered and recycled.[3−24] Although inorganic oxide precursors commonly used in polymer templating procedures (for instance, tetraethyl orthosilicate) are quite expensive, a considerable progress has recently been made in finding their inexpensive alternatives (for instance, sodium silicate).[21−24] A remarkable contribution to the synthesis of polymer-templated ordered porous oxides has been made by Stucky and co-workers, who used triblock copolymer, star diblock copolymer and oligomeric surfactants to obtain mesoporous silicas with several different ordered porous structures.[7] Inspired by the previous developments in the synthesis of ionic-surfactant-templated silicas in the form of films,[25−30] fibers,[31,32] monoliths,[33,34] spheres,[35] and various other morphologies,[31,36,37] the polymer-templated ordered silicas were synthesized as fibers,[8] continuous films,[9] rods,[10] mesoporous-macroporous membranes,[11] monoliths,[12−15] spheres,[16] and many other forms.[16] Triblock-copolymer templating also allowed for the preparation of many periodic large-pore mesoporous oxides,[19] what significantly enhanced the previously recognized opprotunities in the synthesis of non-silica ordered mesoporous oxides (see for instance refs 38 and 39). Moreover, in combination with polystyrene sphere templating and micromolding, the polymer-templating approach was suitable for the preparation of oxides with porous systems independently tailored on three different length scales.[20] Due to its robustness in terms of the synthesis conditions, pore size adjustment capabilities and tailored particle morphology, hexagonally ordered SBA-15 silica[7] is currently the most prominent member of the family of block copolymer templated materials. Numerous applications

* Corresponding author. E-mail: Jaroniec@columbo.kent.edu. Phone: (330) 672 3790. Fax: (330) 672 3816.

10.1021/jp002597a CCC: $19.00
Published on Web 11/02/2000

of SBA-15 in the fields of catalysis, adsorption and advanced materials design can be envisioned. In particular, after soft lithography patterning, SBA-15 was found applicable as a waveguide and mirrorless laser.[40] Following earlier works on the functionalization of ordered mesoporous structures via heteroatom incorporation[1,41−43] and surface modification,[1,44−47] SBA-15 with framework-incorporated Al[48−50] and Ti[51,52] was synthesized, and the SBA-15 surface was functionalized via bonding of organosilanes.[53−56] The resulting functionalized SBA-15 materials exhibited facile catalytic properties,[48−50,53,57] were suitable for adsorption of heavy metal ions,[54] and for sequestration and release of proteins.[55]

In light of these remarkable achievements, the elucidation of structural properties of SBA-15 deserves much attention. In particular, the problem of the possible presence of microporosity[50,52,58,59] and the location of micropores in the SBA-15 structure[59] require careful investigation. The presence of micropores can be deduced from the original data on the SBA-15 structure, which were reported by Stucky and co-workers.[7] Namely, it is clear that SBA-15 does not fulfill a fundamental relation between the structural parameters for materials with uniform pores of simple circular or hexagonal geometry: $wS/V = 4$ or 4.2, respectively (w, S and V are the pore size, pore volume, and surface area, respectively). SBA-15 samples, for which adsorption data were originally reported[7] (and thus the possibility of any significant errors due to the presence of secondary mesopores can be ruled out), exhibited the wS/V ratios between 5.8 and 10.8, which is far from the aforementioned theoretical values. This observation suggested us that the specific surface area of SBA-15 is far too large for a material with approximately cylindrical uniform pores of such size and volume, which in turn indicated the presence of additional smaller pores, possibly micropores (the latter are defined here as pores of diameter below 2 nm), which are necessarily disordered, otherwise their presence would be evident from X-ray diffraction (XRD) and transmission electron microscopy (TEM). It should be noted that the pore corrugation and surface roughness are highly unlikely to account for the observed excess (up to about 2.5 times) in the specific surface area, and even if so, such extreme roughness and/or corrugation would almost certainly fall under the definition of porosity (micro- or mesoporosity).[60] Stucky and co-workers reported that nitrogen adsorption data provide evidence for microporosity of SBA-15 (although they did not discuss the origin of microporosity and its location in the structure),[58] but later concluded that the adsorption behavior previously observed was primarily attributable to the high surface area of SBA-15 rather than to the presence of any appreciable amounts of micropores.[52] Others concluded on the basis of analysis of nitrogen adsorption isotherms that SBA-15 and Al−SBA-15 are microporous, and microporosity is retained after various hydrothermal and thermal treatments, except for the treatment at pH = 11 at room temperature, which appeared to eliminate the micropores of SBA-15 silica.[50] In this study, the location and origin of micropores were also not discussed.

In this contribution, we provide unambiguous evidence for the presence of micropores and connectivity of ordered mesopores in the SBA-15 samples, which were synthesized as reported by Stucky et al.[7] using the most common triblock copolymer template (Pluronic P123).[7−16,19,20,23,40,48−59] The microporosity was evident from nitrogen adsorption data for calcined SBA-15 samples on the basis of the α_s plot analysis, pore size distributions, and excessive values of the wS/V ratios. The changes in porosity of SBA-15 caused by thermal treatment up to 1273 K were analyzed and the evidence of the retention of complementary pores up to 1173 K is provided, whereas the treatment at 1273 K led most likely to a complete elimination of these pores, thus rendering the SBA-15 sample with adsorption properties highly similar to those of large-pore MCM-41. The adsorption-based assessment of the complementary pore size is further corroborated and refined by employing a selective pore blocking via chemical bonding of organosilanes. This methodology has not been used before in studies of porosity of ordered mesoporous materials. The evidence of connectivity between large-pore SBA-15 channels is provided by employing a novel methodology proposed herein, which involves the examination of inverse platinum replicas of the ordered mesoporous structure. Finally, the formation of the connecting micropores is related to the properties of triblock copolymer templates used for the synthesis of SBA-15. The conclusions of this work were further corroborated and discussed in our subsequent XRD, nitrogen adsorption and thermogravimetric study of water-washed, ethanol-washed and calcined SBA-15.[59]

2. Materials and Methods

2.1. Materials. SBA-15 samples were synthesized at 318 K and then heated at 353 K for 1 day (sample A) or 373 K for 2 days (sample B) following the procedure reported by Stucky and co-workers.[7] The details of the synthesis procedure used and the results of XRD, nitrogen adsorption and thermogravimetric analysis of these samples were described elsewhere.[59] As shown therein, XRD patterns and nitrogen adsorption isotherms for the calcined samples as well as the unit-cell sizes, pore volumes, and specific surface areas were similar to those of the corresponding materials described by Stucky and co-workers, and indicative of high-quality SBA-15. Highly ordered MCM-41 sample used for comparison was synthesized using docosyltriethylammonium surfactant, as reported elsewhere along with the results of the detailed characterization using TEM, XRD, nitrogen adsorption and thermogravimetry (TGA).[61]

The SBA-15 and MCM-41 samples were modified via chemical bonding with octyldimethylsilyl (ODMS) groups. SBA-15 sample A was also modified with trimethylsilyl (TMS) groups. The details of the modification are similar to those reported in our previous studies.[62,63] A typical synthesis involved dispersion of 0.2 g of the calcined mesoporous material (without initial treatment) in 2.5 mL of alkyldimethylchlorosilane (alkyl = octyl or methyl) followed by addition of 15 mL of anhydrous pyridine that was used as a solvent. The mixture was refluxed (about 393 K) for 24 h and after cooling, the modified mesoporous material was washed many times on the glass filter with small portions of toluene, isopropyl alcohol, and heptane to remove an excessive amount of modifier, pyridine and possible products of hydrolysis. Finally, the sample was dried overnight in an oven (368−373 K) under vacuum. The surface coverage of bonded groups was 2.48, 2.14 and 2.33 μmol m^{-2} for SBA-15 A-TMS, A-ODMS and B-ODMS, and 2.50 μmol m^{-2} for MCM-41 ODMS (calculated on the basis of the carbon content and BET specific surface area of unmodified samples).

The preparation of inverse platinum replicas of SBA-15 for TEM imaging was carried out as follows. Platinum was incorporated in SBA-15 channels according to the procedure reported elsewhere.[64,65] The Pt/SBA-15 sample was washed with 10 wt % hydrofluoric acid to dissolve the silica template. The resultant black-colored powder Pt sample was allowed to settle by centrifugation. After the supernatant solution was discarded, the Pt sample was diluted with ethanol. The ethanol suspension containing the Pt particles was dropped on TEM grid, and the volatiles were allowed to evaporate.

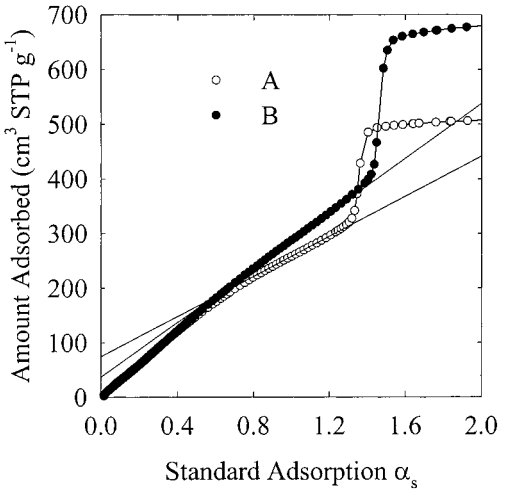

Figure 1. α_s plots for SBA-15 silicas.

2.2. Measurements. Nitrogen and argon adsorption isotherms were measured at 77 K on a Micromeritics ASAP 2010 volumetric adsorption analyzer. Carbon content was determined using a LECO CHNS-932 elemental analyzer. TEM images were obtained using a Philips CM20 transmission electron microscope operated at 100 kV. For thermal stability studies, SBA-15 sample previously calcined at 823 K was heated to 973 K with the initial heating ramp of 2 K min^{-1} and kept at 973 K for 4 h. The same sample was further calcined at 1073, 1173, and 1273 K using the same heating ramp and time. Each of these heat treatments was followed by nitrogen adsorption studies.

2.3. Methods. The specific surface area was assessed from nitrogen adsorption data in the relative pressure range from 0.04 to 0.2 using the standard BET method.[60] The primary mesopore volume, external surface area and micropore volume were determined using the α_s plot method[60] as described in detail elsewhere.[59,61] The reference adsorption isotherm for silicas[66] was used in α_s plot analysis of the unmodified silicas and the TMS-modified sample, whereas the reference adsorption isotherm for ODMS-modified silicas was used in analysis of ODMS-modified materials.[67] Pore size distributions were calculated using the BJH algorithm[68] with the relation between the pore size and the capillary condensation pressure calibrated using MCM-41 silicas.[69] In the BJH calculations, the statistical film thickness curve (t-curve) for silicas[66,69] was used for unmodified and TMS-modified samples, whereas the t-curve for ODMS-modified silicas was used for ODMS-modified samples.

3. Results and Discussion

As expected from the results reported by Stucky and co-workers,[7] the structural parameters of the SBA-15 samples studied herein exhibited large deviations from those characteristic of cylindrical or hexagonal pores ($wS/V = 7.6$ and 7.2, respectively, for samples A and B; V and S are defined here as the volume and specific surface area of primary mesopores and any other pores of diameters smaller than that of the latter). The initial parts of the α_s plots calculated from nitrogen adsorption data using a reliable reference adsorption isotherm for amorphous silica[66] were appreciably nonlinear (Figure 1), thus revealing the presence of micropores, whose volume was estimated as about 0.12 and 0.06 cm^3 g^{-1}, respectively, for samples A and B.[59] The initial parts of the α_s-plots did not exhibit any steps, which in this case is indicative of broad pore size distributions (PSDs) in the micropore/small-mesopore range. PSDs for the SBA-15 samples calculated using the procedure carefully calibrated and validated on high-quality MCM-41 samples[69] confirmed that the uniform large pores of SBA-15 are accompanied by a broad distribution of significantly narrower pores with the maximum at about 2 nm (Figures 2 and 3). In addition, the calculations suggested a continuous PSD from the micropore range up to the range corresponding to the primary mesopores. This was further investigated by examining the adsorption behavior of the samples in the region of adsorption−desorption hysteresis. Hysteresis loops on nitrogen adsorption isotherms for the SBA-15 samples under study exhibited closure points well above 0.4, the latter being the lower limit of adsorption−desorption hysteresis in the case of nitrogen adsorption at 77 K. This indicated the absence of pores which would exhibit hysteresis in the pressure range from the lower closure point of the hysteresis loop to the lower limit of hysteresis, which in this case corresponds to pores of size down to 4.2 nm in diameter. This suggested the absence of complementary porosity of the size above 4.2 nm. This conclusion was further corroborated on the basis of argon adsorption isotherms measured at 77 K. In this case, adsorption−desorption hysteresis can be observed for pores of diameter larger than ca. 3.4 nm (relative pressures down to about 0.27).[70] For the SBA-15 samples under study, hysteresis loops were observed only in

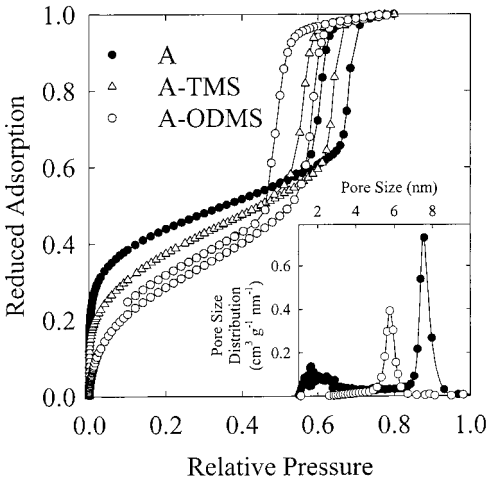

Figure 2. Reduced nitrogen adsorption isotherms for the SBA-15 sample A, unmodified and chemically modified with TMS and ODMS ligands. The inset shows the corresponding pore size distributions.

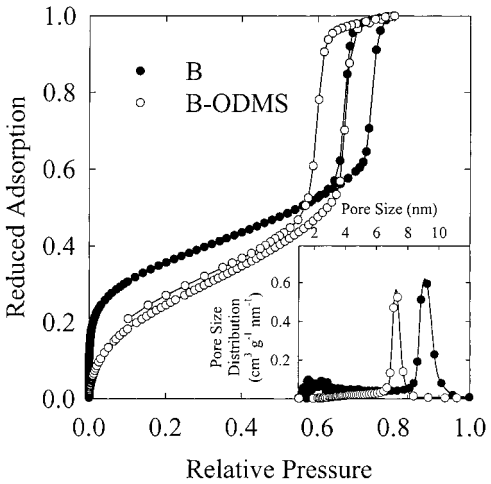

Figure 3. Reduced nitrogen adsorption isotherms for the SBA-15 sample B, unmodified and chemically modified with ODMS ligands. The inset shows the corresponding pore size distributions.

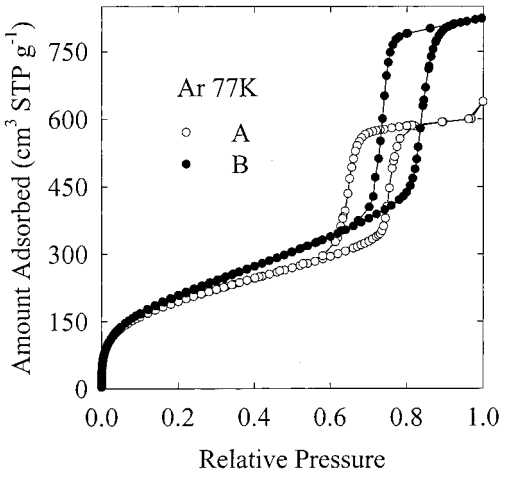

Figure 4. Argon adsorption isotherms measured at 77 K for the SBA-15 samples under study.

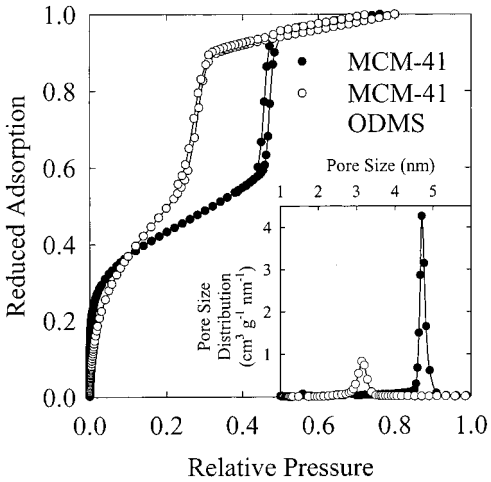

Figure 5. Reduced nitrogen adsorption isotherms for the MCM-41 silica, unmodified and chemically modified with ODMS ligands. The inset shows the corresponding pore size distributions.

the relative pressure range corresponding to the capillary condensation/evaporation in primary mesopores (above about 0.6, see Figure 4), thus indicating the absence of complementary pores of the size exceeding 3.4 nm and artificial nature of tails on PSDs for pore sizes from 3.4 up to about 6.5 nm. The appearance of such artificial tails is rather unexpected, since PSDs calculated for large-pore MCM-41 using the methodology employed herein (which assumes the presence of approximately cylindrical pores) do not feature such artificial tails. Since the tails cannot be attributed to the actual porosity or to the incorrect calculation procedure, they may be related to the deviations from the approximately cylindrical pore geometry, perhaps to the pore roughness and/or corrugation.

To provide an independent confirmation of the presence of the complementary micropores/mesopores, calcined SBA-15 was modified via chemical bonding of relatively small trimethylsilyl (TMS) and large octyldimethylsilyl (ODMS) ligands. The modification of SBA-15 with large ODMS ligands brought about a dramatic decrease in the BET specific surface area (from 780 to 210 and from 850 to 290 $m^2\ g^{-1}$ in the case of samples A and B, respectively). The corresponding decrease in the BET specific surface area was much smaller in the case of ODMS-modified MCM-41 (from 1000 to 440 $m^2\ g^{-1}$) despite its comparable surface coverage with bonded ligands. In the case of SBA-15, a significant lowering of the BET surface area (from 780 to 450 $m^2\ g^{-1}$) was also observed after surface modification with relatively small TMS groups. The resulting changes in the adsorption properties were particularly striking on the reduced adsorption curves (adsorption isotherms divided by the amount adsorbed at a relative pressure of 0.8), which reflect the surface area/pore volume ratios, since the reduced adsorption below the capillary condensation step is proportional to the specific surface area per unit pore volume. It can be seen that the surface area/pore volume ratio significantly decreased upon the modification (see Figures 2 and 3), although an opposite effect can be expected for cylindrical pores, whose size decreased as a result of the modification (see for instance data for MCM-41[1] shown in Figure 5). The values of *wS*/*V* for ODMS-modified SBA-15 samples A and B were 4.1 and 4.2, respectively, similar to the value of 4.1 for ODMS-modified MCM-41. The value of *wS*/*V* was 6.0 for TMS-modified sample. This shows that the complementary pores of SBA-15 were effectively blocked by long-chain ODMS ligands (see also PSDs in Figures 2 and 3), whereas TMS groups were too small and blocked only a certain fraction of these pores. This indicates that a significant fraction of the complementary pores of SBA-15 exhibits sizes between 1 and 3 nm (the latter limits being imposed by the size of TMS and ODMS ligands[59]) and there is essentially no complementary pores of the size above about 3 nm. Therefore, the results of the surface modification of SBA-15 are consistent with the conclusions from the analysis of nitrogen and argon adsorption−desorption hysteresis behavior and provide confirmation of the general correctness of the PSDs shown in Figures 2 and 3, with exception of the tailing between the two prominent peaks on these PSDs. It should be noted that these results cannot be explained when one assumes that the excessive *wS*/*V* ratio for SBA-15 is related with its surface roughness and/or corrugation. While one can envision the masking of such surface features by rather long and flexible ODMS ligands, these features cannot be masked to any appreciable extent by small and rigid TMS groups. It also should be noted that hysteresis loops for unmodified SBA-15 are rather narrow, which is difficult to reconcile with the idea of the prominent surface roughness/corrugation, since these features would be likely to cause a pronounced pore necking effect, which would in turn lead to the broadening of hysteresis loops. Moreover, the width of the hysteresis loops for SBA-15 did not change appreciably as a result of the modification, which suggests that the modification may preserve the pore corrugation, if there is any. Therefore, our characterization procedure based on the blocking of pores with ligands of purposefully chosen size provides an unequivocal evidence for the presence of complementary porosity (that is micropores and mesopores of the size up to about 3 nm) in the SBA-15 samples synthesized by employing the most commonly used procedure.

To determine the location of the complementary porosity, platinum was deposited inside the SBA-15 pores. The resulting platinum nanostructures were isolated via dissolution of the SBA-15 framework and imaged using TEM (images were taken also for Pt/SBA-15 composites). For loadings below 5 wt %, Pt was observed in the form of dots. When the loading was increased to about 10%, dots, single wires and bundles were observed. Above 30% loading, bundles were most often observed. TEM image of one of such self-standing platinum bundles obtained via SBA-15 templating is shown in Figure 6. This nanostructure was a large bundle of parallel wires of the diameter consistent with the size of the ordered pores of SBA-15, and separated by the repeating distance corresponding to that in the structure of the SBA-15 template. In contrast, platinum nanowires prepared in MCM-41 pores did not agglomerate readily, and even when the agglomerates were

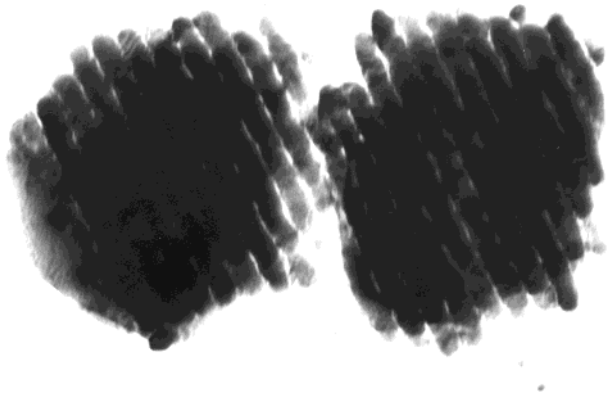

Figure 6. TEM image of the inverse platinum replica of the SBA-15 sample B.

observed, there was no uniform repeating distance between the adjacent nanowires in the agglomerates. These results demonstrate that the self-agglomeration of separate platinum nanowires in ordered bundles is not observed and most likely virtually impossible under the conditions employed in our study. Therefore, the formation of ordered bundles of Pt nanowires using SBA-15 template provided an unequivocal evidence that ordered mesopores of SBA-15 are interconnected, which in combination with the other results discussed above strongly indicates that the complementary micropores/mesopores are located in the walls of ordered mesopores and provide connectivity between them. It should be noted that the pore wall thickness of the SBA-15 samples under study was estimated to be about 2 nm on the basis of XRD and nitrogen adsorption data.[59] Using geometrical considerations advanced elsewhere,[71] one can demonstrate that such a pore wall thickness is sufficient to house complementary pores in the amount of about 0.1 cm^3 g^{-1}, or even higher. At the same time, the separation between the wires in the bundles observed by TEM is rather small in comparison to the diameter of the platinum nanowires. It also needs to be kept in mind that the connections between nanowires are distributed in a disordered way, since they are formed in confines of disordered complementary pores. TEM images are projections along the incident beam direction, and thus the image of the aligned nanowires in the bundle is expected to produce much better contrast than the disordered connections between nanowires. Because of that, the connections between nanowires in the bundles can readily escape the imaging capability of the TEM used, although some evidence of the connections was actually observed (see Figure 6). However, the very formation of the ordered bundles would be virtually impossible without such connections, as demonstrated on the example of the MCM-41 templating of Pt nanostructures.

The formation of the connecting pores is most likely related to the hydrophilic nature of EO-blocks of the triblock copolymer template,[5,7,76,77] which leads to the formation of the silica framework around the EO-blocks,[7] thereby incorporating them in the pore walls. To this end, it was already suggested that EO-blocks may be occluded in the framework of triblock copolymer templated silicas.[12] Moreover, organoaluminosilicate materials templated using diblock copolymers were shown to exhibit intimate mixing of the inorganic phase and EO blocks.[77] Since EO-blocks of adjacent micelles may be highly entangled,[78] the penetration of EO-blocks within the pore walls of as-synthesized SBA-15 may provide connectivity between the cylindrical micellar templates, and consequently, between the pores of the calcined materials.

The thermal stability of SBA-15 structure and its complementary porosity in particular was investigated using nitrogen

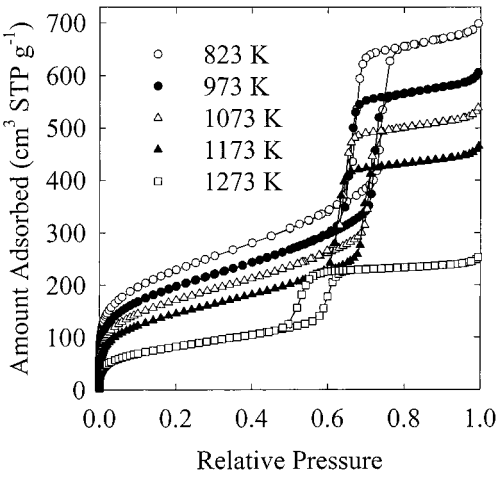

Figure 7. Nitrogen adsorption isotherms for the SBA-15 sample B calcined at 823 K and subsequently heated at temperatures up to 1273 K.

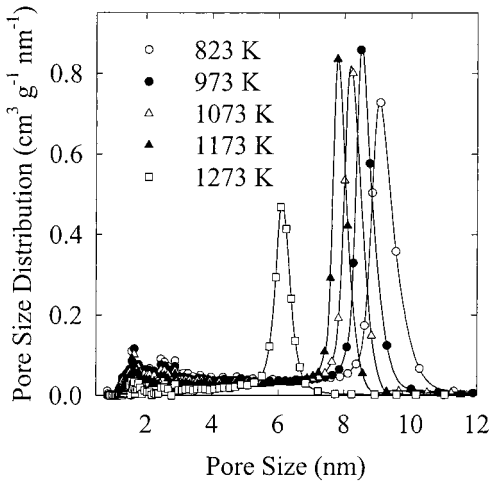

Figure 8. Pore size distributions for the SBA-15 sample B calcined at 823 K and subsequently heated at temperatures up to 1273 K.

adsorption. For this purpose, nitrogen adsorption isotherm for sample B was acquired once again (Figure 7) to make sure that the storage (about 1.5 years) did not change its properties. Minor pore volume and specific surface area lowering was observed (about 3%), and the sample exhibited somewhat stronger low-pressure adsorption. We have observed a similar behavior in the case of MCM-41 and it can be attributed to rehydroxylation of the silica surface upon storage. However, the storage did not have any detrimental effect on the uniformity of pore size of the material (compare Figure 3 with Figure 8), although the *wS*/*V* ratio slightly dropped to 7.1. After having assured that the storage did not have any appreciable effect on the properties of the SBA-15 sample, we subjected it to high-temperature calcination. The latter resulted in a significant decrease in the specific surface area from 830 to 720, 620, 530, and 300 m^2 g^{-1}, and in the pore volume (the sum of primary mesopore and complementary pore volume) from 0.96 to 0.83, 0.73, 0.63, and 0.34 cm^3 g^{-1}, after calcination at 973, 1073, 1173, and 1273 K, respectively. MCM-41 samples subjected to similar high-temperature treatments sometimes retained much larger specific surface areas and comparable pore volumes.[72−74] However, the reported data suggest that MCM-41 lost the uniformity of its pore structure after high-temperature calcination.[73,74] In contrast, calcination at 973−1173 K appears to improve the uniformity of the pore size of SBA-15. Whether this was actually the case, or the narrowing of the PSD resulted from gradual elimination

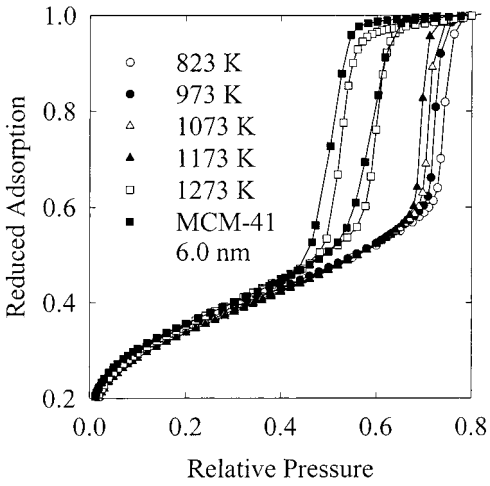

Figure 9. Reduced adsorption curves for the SBA-15 sample B calcined at 823 K and subsequently heated at temperatures up to 1273 K. For heat treatments below 1273 K, only adsorption branches of adsorption isotherms are shown. Data for a large-pore MCM-41 are provided for comparison.

of complementary pores and possibly smoothing off the surface corrugation/roughness, remains to be further investigated. XRD data suggest that SBA-15 calcined at high temperature was still well-ordered, but not as uniform as that calcined at 823 K.

Because of the fact that high-temperature calcination leads to prominent dehydroxylation thereby altering the surface properties and consequently low-pressure adsorption properties of silicas,[75] it was difficult to reliably determine the micropore volume by the α_s plot analysis. Nonetheless, the latter method clearly indicated microporosity for samples calcined at 973 and 1073 K. However, the alteration in the surface properties caused by the silica surface dehydroxylation is not likely to have any significant effect on the values of *wS*/*V* ratios, and therefore the latter are suitable for the monitoring of evolution of the complementary porosity and surface corrugation/roughness during the heat treatment. We found that the *wS*/*V* ratio dropped to 6.7, 6.3, 5.9, and 5.0 after calcination at 973, 1073, 1173, and 1273 K, respectively. The ratio attained after calcination at 1273 K is close to that for MCM-41 (MCM-41 samples[69] with pore sizes of about 6.1 nm, which are comparable to that of SBA-15 calcined at 1273 K, exhibited the *wS*/*V* ratios of 4.9 and 5.0, whereas the MCM-41 sample with the pore size of 4.8 nm used in the current study for comparison had the ratio of 4.6). It should be noted here that the BET specific surface area is significantly overestimated for silicas, but quite accurate for ODMS-modifed silicas (see ref 67 and references therein), which is primarily responsible for deviations from the theoretical ratio of 4.0−4.2 for MCM-41 pores when the BET specific surface area is used for calculations. As expected, such deviations were not observed for ODMS-modified samples.

We thus obtained SBA-15 silica with pore structure properties similar to those of MCM-41 (see reduced adsorption curves in Figure 9). The transition from the structure with anomalously high specific surface area to that with properties similar to MCM-41 provides additional evidence that the structure of SBA-15 prepared under standard conditions is significantly different from that of MCM-41, as argued in the current study. Our results also prove that SBA-15 is exceptionally thermally stable. Highly ordered porosity was retained after calcination at 1273 K (porosity of MCM-41 treated under similar conditions was rather poorly ordered[73,74]) and the degree of pore size uniformity was still higher than that of large-pore MCM-41 synthesized using the postsynthesis hydrothermal treatment at 423 K.[69] It can be speculated that the presence of complementary pores may help relieve the stress caused by the shrinkage under high-temperature conditions and may hinder the propagation of structural defects.

After the original submission of this work and our related work on XRD, nitrogen adsorption and thermogravimetric characterization of SBA-15,[59] the preparation of noble metal nanostructures in ordered mesoporous and macroporous materials received much attention, which manifested itself in the submission of three contributions strongly related to our work, which were already made available to the scientific community.[79−81] Yang and co-workers reported the synthesis of silver nanowires in pores of SBA-15, although the resulting noble metal nanostructures were not isolated from the silica template.[79] Stucky and co-workers reported the synthesis of gold, platinum and silver nanowires in SBA-15 pores, and their subsequent isolation via dissolution of the SBA-15 template.[80] Although these authors reported that they were able to avoid bulk agglomeration of metal, they used relatively low loadings (for instance 5% of Pt) to attain clear TEM images and still the reported images of the nanowires indicate that it is difficult to obtain separate Pt wires. In particular, one of the images showed one separate Pt nanowire and the second nanowire with a short adjacent nanowire attached to it, whereas the second image showed a bundle of uniformly arranged Pt nanowires spaced with a distance similar to that between the adjacent pores of SBA-15 template (the latter can be estimated from the provided XRD pattern). So, the data in ref 80 provide an additional confirmation of our results reported herein, which were originally submitted for publication before those by Stucky at al.[80] In addition, Mallouk et al. reported the synthesis of platinum nanostuctures using colloidal crystals as templates.[81]

4. Conclusions

The porous structure of SBA-15 consists not only of large, uniform, and ordered channels (as known before) but also of much smaller complementary pores (which was suggested before by one research group, and suggested and then discounted by the second one), which provide connectivity between the ordered channels (which was not known before). The complementary pores appear to be stable up to 1173 K, but calcination at 1273 K appears to eliminate them and allows one to obtain the SBA-15 sample with adsorption (and thus porous structure) properties close to those of MCM-41. Since the formation of the complementary pores appears to be related to the inherent properties of the triblock copolymer template with EO-blocks, many other materials templated by copolymers may also exhibit structures with large mesopores accompanied by and/or connected via smaller pores. The presence of microporosity and the connectivity of the large uniform mesopores of polymer templated silicas, and perhaps other porous oxides, may have a significant impact on the potential applications of these remarkable materials. Moreover, the possibility of elimination of the complementary pores via the heat treatment may greatly enhance our ability to fine-tune the structures of polymer-templated mesoporous silicas, and perhaps, other mesoporous oxides. Finally, the methods proposed herein based on the selective pore blocking via surface modification and on the preparation of inverse platinum replicas promise to be highly useful in the elucidation of structures of ordered mesoporous materials.

Note Added in Proof. The conclusion about connectivity of ordered SBA-15 pores via complementary pores in the siliceous walls has been recently additionally confirmed by a successful SBA-15-templated synthesis of hexagonally ordered mesoporous carbon with the structure consistent of uniformly spaced rods (*J. Am. Chem. Soc.* **2000**, *122*, 10712).

Acknowledgment. The donors of the Petroleum Research Fund administrated by the American Chemical Society are gratefully acknowledged for partial support of this research. One of the Reviewers of this paper is acknowledged for his/her suggestion to study the thermal stability of SBA-15 structure.

References and Notes

(1) Kresge, C. T.; Leonowicz, M. E.; Roth, W. J.; Vartuli, J. C.; Beck, J. S. *Nature* **1992**, *359*, 710.

(2) Yanagisawa, T.; Shimizu, T.; Kuroda, K.; Kato, C. *Bull. Chem. Soc. Jpn.* **1990**, *63*, 988.

(3) Attard, G. S.; Glyde, J. C.; Goltner, C. G. *Nature* **1995**, *378*, 366.

(4) Bagshaw, S. A.; Prouzet, E.; Pinnavaia, T. J. *Science* **1995**, *269*, 1242.

(5) Goltner, C. G.; Berton, B.; Kramer, E.; Antonietti, M. *Adv. Mater.* **1999**, *11*, 395.

(6) Lu, Y.; Fan, H.; Stump, A.; Ward, T. L.; Rieker, T.; Brinker, J. C. *Nature* **1999**, *398*, 223.

(7) Zhao, D.; Huo, Q.; Feng, J.; Chmelka, B. F.; Stucky, G. D. *J. Am. Chem. Soc.* **1998**, *120*, 6024.

(8) Yang, P.; Zhao, D.; Chmelka, B. F.; Stucky, G. D. *Chem. Mater.* **1998**, *10*, 2033.

(9) Zhao, D.; Yang, P.; Melosh, N.; Feng, J.; Chmelka, B. F.; Stucky, G. D. *Adv. Mater.* **1998**, *10*, 1380.

(10) Schmidt-Winkel, P.; Yang, P.; Margolese, D. I.; Chmelka, B. F.; Stucky, G. D. *Adv. Mater.* **1999**, *11*, 303.

(11) Zhao, D.; Yang, P.; Chmelka, B. F.; Stucky, G. D. *Chem. Mater.* **1999**, *11*, 1174.

(12) Melosh, N. A.; Lipic, P.; Bates, F. S.; Wudl, F.; Stucky, G. D.; Fredrickson, G. H.; Chmelka, B. F. *Macromolecules* **1999**, *32*, 4332.

(13) Feng, P.; Bu, X.; Stucky, G. D.; Pine, D. J. *J. Am. Chem. Soc.* **2000**, *122*, 994.

(14) Melosh, N.; Davidson, P.; Chmelka, B. F. *J. Am. Chem. Soc.* **2000**, *122*, 823.

(15) Feng, P.; Bu, X.; Pine, D. J. *Langmuir* **2000**, *16*, 5304.

(16) Zhao, D.; Sun, J.; Li, Q.; Stucky, G. D. *Chem. Mater.* **2000**, *12*, 275.

(17) Yu, C.; Yu, Y.; Zhao, D. *Chem. Commun.* **2000**, 575.

(18) Yu, Y.; Yu, C.; Yu, Z.; Zhao, D. *Chem. Lett.* **2000**, 504.

(19) Yang, P.; Zhao, D.; Margolese, D. I.; Chmelka, B. F.; Stucky, G. D. *Nature* **1998**, *396*, 152.

(20) Yang, P.; Deng, T.; Zhao, D.; Feng, P.; Pine, D.; Chmelka, B. F.; Whitesides, G. M.; Stucky, G. D. *Science* **1998**, *282*, 2244.

(21) Sierra, L.; Guth, J.-L. *Microporous Mesoporous Mater.* **1999**, *27*, 243.

(22) Kim, S.-S.; Pauly, T. R.; Pinnavaia, T. J. *Chem. Commun.* **2000**, 835.

(23) Kim, J. M.; Stucky, G. D. *Chem. Commun.* **2000**, 1159.

(24) Boissiere, C.; Larbot, A.; Prouzet, E. *Chem. Mater.* **2000**, *12*, 1937.

(25) Yang, H.; Kuperman, A.; Coombs, N.; Mamiche-Afara, S.; Ozin, G. A. *Nature* **1996**, *379*, 703.

(26) Aksay, I. A.; Trau, M.; Manne, S.; Honma, I.; Yao, N.; Zhou, L.; Fenter, P.; Eisenberger, P. M.; Gruner, S. M. *Science* **1996**, *273*, 892.

(27) Ogawa, M. *Chem. Commun.* **1996**, 1149.

(28) Lu, Y.; Ganguli, R.; Drewien, C. A.; Anderson, M. T.; Brinker, C. J.; Gong, W.; Guo, Y.; Soyez, H.; Dunn, B.; Huang, M. H.; Zink, J. I. *Nature* **1997**, *389*, 364.

(29) Ryoo, R.; Ko, C. H.; Cho, S. J.; Kim, J. M. *J. Phys. Chem. B* **1997**, *101*, 10610.

(30) Tolbert, S. H.; Schaffer, T. E.; Feng, J.; Hansma, P. K.; Stucky, G. D. *Chem. Mater.* **1997**, *9*, 1962.

(31) Schacht, S.; Huo, Q.; Voigt-Martin, I. G.; Stucky, G. D.; Schuth, F. *Science* **1996**, *273*, 768.

(32) Bruinsma, P. J.; Kim, A. Y.; Liu, J.; Baskaran, S. *Chem. Mater.* **1997**, *9*, 2507.

(33) Anderson, M. T.; Martin, J. E.; Odinek, J. G.; Newcomer, P. P.; Wilcoxon, J. P. *Microporous Mater.* **1997**, *10*, 13.

(34) Tolbert, S. H.; Firouzi, A.; Stucky, G. D.; Chmelka, B. F. *Science* **1997**, *278*, 264.

(35) Grun, M.; Lauer, I.; Unger, K. K. *Adv. Mater.* **1997**, *9*, 254.

(36) Lin, H.-P.; Mou, C.-Y. *Science* **1996**, *273*, 765.

(37) Yang, H.; Coombs, N.; Ozin, G. A. *Nature* **1997**, *386*, 692.

(38) Antonelli, D. M.; Ying, J. Y. *Angew. Chem., Int. Ed. Engl.* **1996**, *35*, 426.

(39) Tian, Z.-R.; Tong, W.; Wang, J.-Y.; Duan, N.-G.; Krishnan, V. V.; Suib, S. L. *Science* **1997**, *276*, 926.

(40) Yang, P.; Wirnsberger, G.; Huang, H. C.; Cordero, S. R.; McGehee, M. D.; Scott, B.; Deng, T.; Whitesides, G. M.; Chmelka, B. F.; Buratto, S. K.; Stucky, G. D. *Science* **2000**, *287*, 465.

(41) Corma, A.; Navarro, M. T.; Perez Pariente, J. *J. Chem. Soc., Chem. Commun.* **1994**, 147.

(42) Tanev, P. T.; Chibve, M.; Pinnavaia, T. J. *Nature* **1994**, *368*, 321.

(43) Reddy, K. M.; Moudrakovski, I.; Sayari, A. *J. Chem. Soc., Chem. Commun.* **1994**, 1059.

(44) Brunel, D.; Cauvel, A.; Fajula, F.; DiRenzo, F. *Stud. Surf. Sci. Catal.* **1995**, *97*, 173.

(45) Diaz, J. F.; Balkus, K. J., Jr. *J. Mol. Catal. B: Enzymatic* **1996**, *2*, 115.

(46) Feng, X.; Fryxell, G. E.; Wang, L. Q.; Kim, A. Y.; Liu, J.; Kemner, K. *Science* **1997**, *276*, 923.

(47) Mercier, L.; Pinnavaia, T. J. *Adv. Mater.* **1997**, *9*, 500.

(48) Cheng, M.; Wang, Z.; Sakurai, K.; Kumata, F.; Saito, T.; Komatsu, T.; Yashima, T. *Chem. Lett.* **1999**, 131.

(49) Yue, Y.; Gedeon, A.; Bonardet, J.-L.; Melosh, N.; D'Espinose, J.-B.; Fraissard, J. *Chem. Commun.* **1999**, 1967.

(50) Yue, Y.-H.; Gedeon, A.; Bonardet, J.-L.; d'Espinose, J. B.; Melosh, N.; Fraissard, J. *Stud. Surf. Sci. Catal.* **2000**, *129*, 209.

(51) Luan, Z.; Maes, E. M.; van der Heide, P. A. W.; Zhao, D.; Czernuszewicz, R. S.; Kevan, L. *Chem. Mater.* **1999**, *11*, 3680.

(52) Morey, M. S.; O'Brien, S.; Schwarz, S.; Stucky, G. D. *Chem. Mater.* **2000**, *12*, 898.

(53) Bae, S. J.; Kim, S.-W.; Hyeon, T.; Kim, B. M. *Chem. Commun.* **1999**, 31.

(54) Liu, A. M.; Hidajat, K.; Kawi, S.; Zhao, D. Y. *Chem. Commun.* **2000**, 1145.

(55) Han, Y.-J.; Stucky, G. D.; Butler, A. *J. Am. Chem. Soc.* **1999**, *121*, 9897.

(56) Lin, H.-P.; Yang, L.-Y.; Mou, C.-Y.; Liu, S.-B.; Lee, H.-K. *New J. Chem.* **2000**, *24*, 253.

(57) Kim, S.-W.; Son, S. U.; Lee, S. I.; Hyeon, T.; Chung, Y. K. *J. Am. Chem. Soc.* **2000**, *122*, 1550.

(58) Lukens, W. W., Jr.; Schmidt-Winkel, P.; Zhao, D.; Feng, J.; Stucky, G. D. *Langmuir* **1999**, *15*, 5403.

(59) Kruk, M.; Jaroniec, M.; Ko, C. H.; Ryoo, R. *Chem. Mater.* **2000**, *12*, 1961.

(60) Rouquerol, J.; Avnir, D.; Fairbridge, C. W.; Everett, D. H.; Haynes, J. H.; Pernicone, N.; Ramsay, J. D. F.; Sing, K. S. W.; Unger, K. K. *Pure Appl. Chem.* **1994**, *66*, 1739.

(61) Kruk, M.; Jaroniec, M.; Sakamoto, Y.; Terasaki, O.; Ryoo, R.; Ko, C. H. *J. Phys. Chem. B* **2000**, *104*, 292.

(62) Jaroniec, C. P.; Kruk, M.; Jaroniec, M.; Sayari, A. *J. Phys. Chem. B* **1998**, *102*, 5503.

(63) Antochshuk, V.; Jaroniec, M. *J. Phys. Chem. B* **1999**, *103*, 6252.

(64) Ko, C. H.; Ryoo, R. *Chem. Commun.* **1996**, 2467.

(65) Ryoo, R.; Ko, C. H., presented at IUPAC Workshop on Advanced Materials: Nanostructured Systems, Hong Kong, July 14−18, 1999.

(66) Jaroniec, M.; Kruk, M.; Olivier, J. P. *Langmuir* **1999**, *15*, 5410.

(67) Kruk, M.; Antochshuk, V.; Jaroniec, M.; Sayari, A. *J. Phys. Chem. B* **1999**, *103*, 10670.

(68) Barrett, E. P.; Joyner, L. G.; Halenda, P. P. *J. Am. Chem. Soc.* **1951**, *73*, 373.

(69) Kruk, M.; Jaroniec, M.; Sayari, A. *Langmuir* **1997**, *13*, 6267.

(70) Kruk, M.; Jaroniec, M. Unpublished work.

(71) Kruk, M.; Jaroniec, M.; Sayari, A. *Chem. Mater.* **1999**, *11*, 492.

(72) Namba, S.; Mochizuki, A. *Res. Chem. Intermed.* **1998**, *24*, 561.

(73) Chen, L.; Horiuchi, T.; Mori, T.; Maeda, K. *J. Phys. Chem. B* **1999**, *103*, 1216.

(74) Mokaya, R. *J. Phys. Chem. B* **1999**, *103*, 10204.

(75) Glinka, Y. D.; Jaroniec, C. P.; Jaroniec, M. *J. Colloid Interface Sci.* **1998**, *201*, 210.

(76) Wanka, G.; Hoffman, H.; Ulbricht, W. *Macromolecules* **1994**, *27*, 4145.

(77) De Paul, S. M.; Zwanziger, J. W.; Ulrich, R.; Wiesner, U.; Spiess, H. W. *J. Am. Chem. Soc.* **1999**, *121*, 5727.

(78) Kramer, E.; Forster, S.; Goltner, C.; Antonietti, M. *Langmuir* **1998**, *14*, 2027.

(79) Huang, M. H.; Choudrey, A.; Yang, P. *Chem. Commun.* **2000**, 1063.

(80) Han, Y.-J.; Kim, J. M.; Stucky, G. D. *Chem. Mater.* **2000**, *12*, 2068.

(81) Egan, G. L.; Yu, J.-S.; Kim, C. H.; Lee, S. J.; Schaak, R. E.; Mallouk, T. E. *Adv. Mater.* **2000**, *12*, 1040.